Yang *et al.*
Chinese Journal of Mechanical Engineering (2024) 37:104
https://doi.org/10.1186/s10033-024-01084-8

Chinese Journal of Mechanical Engineering

ORIGINAL ARTICLE Open Access

Design and Optimization Analysis of an Adaptive Knee Exoskeleton

Xinhua Yang[1], Sheng Guo[1,2*], Peiyi Wang[1], Yifan Wu[1], Lianzheng Niu[1] and Duxin Liu[1]

Abstract

To solve the problem of undesired relative motion of human-machine interaction positions caused by misalignment of the human-machine joints rotation axis of the knee exoskeleton, this study designed an adaptive knee exoskeleton based on a gear-link mechanism (GLM) by considering the human body as a component of the exoskeleton mechanism. Simultaneously, the concept of the wearable area (WA) was proposed, which transformed the operation of aligning the exoskeleton rotation axis with the human knee joint rotation axis into a "face alignment point" in the sagittal plane, reducing the difficulty of aligning the human-machine joint rotation axis. In the kinematic analysis of GLM, the phenomenon of instantaneous movement of the central axis of the human knee joint was considered. Based on the kinematic model, the WA, velocity transfer ratio, and initial position static stiffness of GLM were analyzed. The NSGA-II optimization algorithm was used to optimize the size parameters of GLM, which increased the WA by 18.4%, the average velocity transfer ratio by 4.98%, and the average initial position static stiffness by 6.01%. Finally, the ability of the exoskeleton to absorb movement displacement (MD) was verified through simulation, and the good human-machine kinematic compatibility of the exoskeleton was verified through wearable tests conducted on the initial mechanism principle prototype.

Keywords Adaptive knee exoskeleton, Gear-link mechanism, Wearable area, Optimization, Simulation

1 Introduction

Decline in walking ability is a common problem faced by the elderly. With age, the muscle strength of the elderly gradually decreases, leading to unsteady walking, difficulty in ascending and descending stairs, and trouble standing up after crouching, which greatly affect the quality of life of the elderly. On the other hand, one of the main reasons why patients with lower limb diseases cannot perform basic activities of daily living on their own after surgery is that their neural pathways are blocked, and medical knowledge has shown that repetitive movements can reactivate the neural pathways of patients [1, 2]. Lower limb rehabilitation robots have an active role in helping elderly people and patients with lower limb dysfunction to assist and rehabilitate their lower limbs, helping them regain their ability to walk and improve the problems caused by walking difficulties. Lower limb exoskeleton robot, as a kind of lower limb rehabilitation robot, integrates sensing, control, and other technologies, and shows the characteristics of the intersection fields of bionics, robotics, information and control science, and medicine, etc., which is an interactive robotic system worn on the outside of the human limb or torso, and moves in concert with the human limb to provide support for the human body, provide assistance for the limb, and aid in limb movement, thus enhancing the human body's functionality [3].

However, a problem that cannot be ignored in the use of exoskeleton devices is the misalignment between the axis of the exoskeleton mechanical rotation joint and the

*Correspondence:
Sheng Guo
Shguo@bjtu.edu.cn
[1] School of Mechanical, Electronic and Control Engineering, Beijing Jiaotong University, Beijing 100044, China
[2] Key Laboratory of Vehicle Advanced Manufacturing, Measuring and Control Technology, Ministry of Education, Beijing Jiaotong University, Beijing 100044, China
Full list of author information is available at the end of the article

axis of human joint rotation. If this misalignment occurs, the exoskeleton generates a force/torque on the human body that is undesired for the assisted movement, and this force/torque creates parasitic forces on the human skin, leading to pain or even injury to the human body and ultimately destroying the exoskeleton's assistance [4–8].

The alignment of the rotation axis of the human-machine joint is particularly challenging for the knee joint [9], as the femur and tibia slide during the flexion process [10]. In the design of some knee exoskeletons, researchers have simplified the human knee joint into a 1 degree of freedom (DOF) revolute joint, e.g. Refs. [11–16]. This oversimplification inevitably leads to misalignment of the human-machine joint rotation axis, which is detrimental to the wearer.

Currently, an increasing number of researchers are paying attention to this problem. The solutions adopted are mainly of three types. The first type of method is the design of biomimetic structures, such as Kim et al. [17] who designed a curved guide rail that mimics the shape of the human femur end by capturing the motion of the tibia and femur. There is also the use of gears [9, 18] to simulate the motion of the knee joint. Furthermore, the instantaneous rotation axis of the knee joint is fitted by means of the cross-four-bar mechanism [19–22]. With this biomimetic structural design, the motion of the mechanism is determined as soon as the design is completed. Due to the differences in the shape and size of each person's knee joint bones, the effectiveness of exoskeletons designed with biomimetic knee joint structures in reducing the misalignment of the human-machine joint rotation axis varies from person to person. In addition, the design of this type of structure is similar to the traditional exoskeleton mechanism design, which simplifies the human knee joint into a 1-DOF revolute joint. When aligning the rotation axis of the human-machine joint, when viewed in the sagittal plane, the operation is to align the "point alignment point" between the exoskeleton rotation center point and the human knee joint rotation center point. However, the human knee joint rotation center cannot be accurately identified by the naked eye, so the alignment operation of the rotation axis of the human-machine joints is undoubtedly difficult.

The second type of method is the design of compliant structures, which absorb the misalignment by adding elastic or flexible components to the exoskeleton mechanism. Jun et al. [23, 24] designed a passive knee joint compliant exoskeleton based on a parallel coupled compliant plate mechanism and a pennate elastic band spring structure. This compliant exoskeleton solved the problem of misalignment and provided users with adjustable stiffness relative to knee joint posture. Sui et al. [25] designed a portable spring knee exoskeleton named SpringExo, which uses a spiral spring design and is worn on the human femur and tibia. It can serve as an energy storage device or a quasi-rigid exoskeleton, allowing for alignment of the rotation axis of the human-machine joints without increasing complexity. However, such designs based on compliant structures still generate parasitic forces on the skin surface, affecting the wearing experience.

The third type of method is the design of adaptive structures. The main idea of this type of method is to adaptively compensate for the misalignment of the human-machine joint rotation axis by increasing redundant DOFs. For example, Celebi et al. [26] designed a self-aligning knee joint exoskeleton AssistOn Knee using a Schmidt coupling mechanism. The exoskeleton can automatically align the rotation axis of the human knee joint, achieving perfect alignment between the rotation axis of the human body and the exoskeleton. Lee et al. [27, 28] designed a self-aligning knee exoskeleton by decoupling the rotation and translation of the knee joint. Subsequently, their team proposed the use of several accurately calculated rolling cams to design an adaptive knee exoskeleton [29, 30], which can adapt to changes in the knee joint rotation axis. On this basis, their team also proposed an exoskeleton designed using a rolling joint, two aligned passive joints, four links, and a sliding mechanism [31], which can adapt to the human knee joint in the frontal and sagittal planes. Sarkisian et al. [6, 7] compensated for the impact of misalignment by adding passive DOFs with a prismatic-revolute-revolute (PRR) configuration at the interaction site between the exoskeleton and the human tibia. Li et al. [32] added a passive DOF to the biomimetic knee exoskeleton, allowing the exoskeleton to adapt to changes in the knee joint rotation axis. Although this type of method can effectively solve the problem of misalignment of the rotation axis of the human-machine joints, it does not take into account that the wearing position of the exoskeleton on the human body will affect the adaptive performance of the exoskeleton mechanism.

To this end, this paper proposes a structural design method for an adaptive knee exoskeleton based on the GLM, which can effectively solve the problem of misalignment of the rotation axis of the human-machine joints in the sagittal plane during human knee joint movement. Considering the difficulty of aligning the rotation axis of the human body joint when the exoskeleton is worn, as well as the influence of wearing position on the adaptive capabilities of exoskeletons, we propose the concept of the WA of knee exoskeleton robots: WA is an area of the exoskeleton in the sagittal plane that the wearer needs to align with the center of rotation of the

human knee joint when wearing the exoskeleton. In other words, when people wear the exoskeleton, in the sagittal plane, the operation of aligning the WA with the axis of rotation of the knee joint is the "face alignment point", which greatly reduces the difficulty of aligning the rotation axis of the human-machine joints when wearing the exoskeleton.

The rest of the paper is organized as follows: Section 2 describes the designed adaptive knee exoskeleton based on the GLM. Section 3 establishes and simulates to validation of the kinematic model of the GLM. Section 4 analyzes the WA of the GLM, the velocity transfer ratio, and the static stiffness at the initial position. Section 5 optimizes the dimensions of the exoskeleton. In Section 6, the adaptive ability and human-machine kinematic compatibility of knee exoskeletons were verified through simulation and a mechanism principle prototype, respectively. Finally, conclusions are drawn in Section 7.

2 Wearable Adaptive Knee Exoskeleton

2.1 Design Requirements

Requirements of exoskeleton-assisted range. According to the anatomy of the human lower limb, the forms of motion of the human knee joint include flexion/extension in the sagittal plane, internal/external rotation in the horizontal plane, and abduction/adduction in the frontal plane. Considering the main movement of the knee joint is flexion/extension, with a maximum flexion range of 130°–150° [33]. This is much greater than the internal/external rotation and abduction/adduction movements. Meanwhile, considering reducing the complexity of the overall structure of the exoskeleton. Therefore, this paper only studies the flexion/extension movement of the knee joint in the sagittal plane. Typically, a range of knee flexion angles of 0°~120° is sufficient for most daily activities, so the maximum flexion angle of the knee joint assisted by the knee exoskeleton designed in this paper is at least 120°.

Requirements for comfort/safety of wearing knee joint exoskeletons. In the design process of knee exoskeletons, full consideration should be given to the phenomenon that the rotation axis of the human knee joint changes with the change of rotation angle during the movement process of the human knee joint. The exoskeleton should be able to adapt to changes in the rotation axis of the human knee joint, thereby reducing or eliminating the discomfort caused by misalignment of the rotation axis of the human-machine joints.

Requirements for the convenience of wearing exoskeletons. This is reflected in the convenience of aligning the rotation axis of the human-machine joints. Traditional knee joint exoskeleton robots that simplify the knee joint into 1-DOF require a lot of time to align the rotation axis of the human-machine joints when wearing. However, in reality, it is difficult to find the rotation axis of the knee joint accurately. Manual alignment of the exoskeleton during wearing relies on human estimation, and there are still deviations after manual alignment. Therefore, achieving rapid alignment of the rotation axis of the human-machine joints when wearing exoskeletons is also a problem to be considered in this paper.

2.2 Design Concept

Analyze the mechanism of misalignment of the rotation axis of the human-machine joints of typical knee exoskeletons [9, 18], as shown in Figure 1a. Two gears are fixedly connected to the femur and tibia, and the meshing point of the gears aligns with the instantaneous center of rotation (ICR) of the human knee joint. The principle of reducing the misalignment between the rotation centers of human-machine joints in this design is to make the meshing point trajectory between the two gears coincide with the trajectory of the ICR of the human knee joint as much as possible. If the meshing point of the gear deviates from the ICR of the human body, there will inevitably be movement distance (MD) in the human-machine interaction positions between the exoskeleton and the human body. This MD is the main cause of discomfort or injury to the human body. The solution to eliminate the MD is to enable the exoskeleton to have the ability to absorb the MD of human-machine interaction positions.

The specific manifestation of MD in the sagittal plane is movement in both directions along the leg surface. Therefore, exoskeleton devices require at least three DOFs: one active DOF to assist in human knee joint movement, and two active/passive DOFs to absorb the MD of human-machine interaction positions.

This paper starts from the perspective of absorbing MD, that is, the misalignment of the rotation axis of the human-machine joints has always existed, but the exoskeleton mechanism can absorb the MD caused by the misalignment. The solution proposed is to add an adaptive link to the exoskeleton of a biomimetic mechanism based on gears, as shown in Figure 1b. At this time, the number of DOFs of the exoskeleton mechanism is 3, and the two ends of the adaptive link are respectively hinged with the femur and a gear. After adding an adaptive link, when the MD is generated, the adaptive link can absorb the MD by adjusting the meshing position of the two gears. In addition, at this point:

(1) When wearing, the meshing point trajectory of the gears does not need to coincide with the ICR trajectory of the human knee joint.

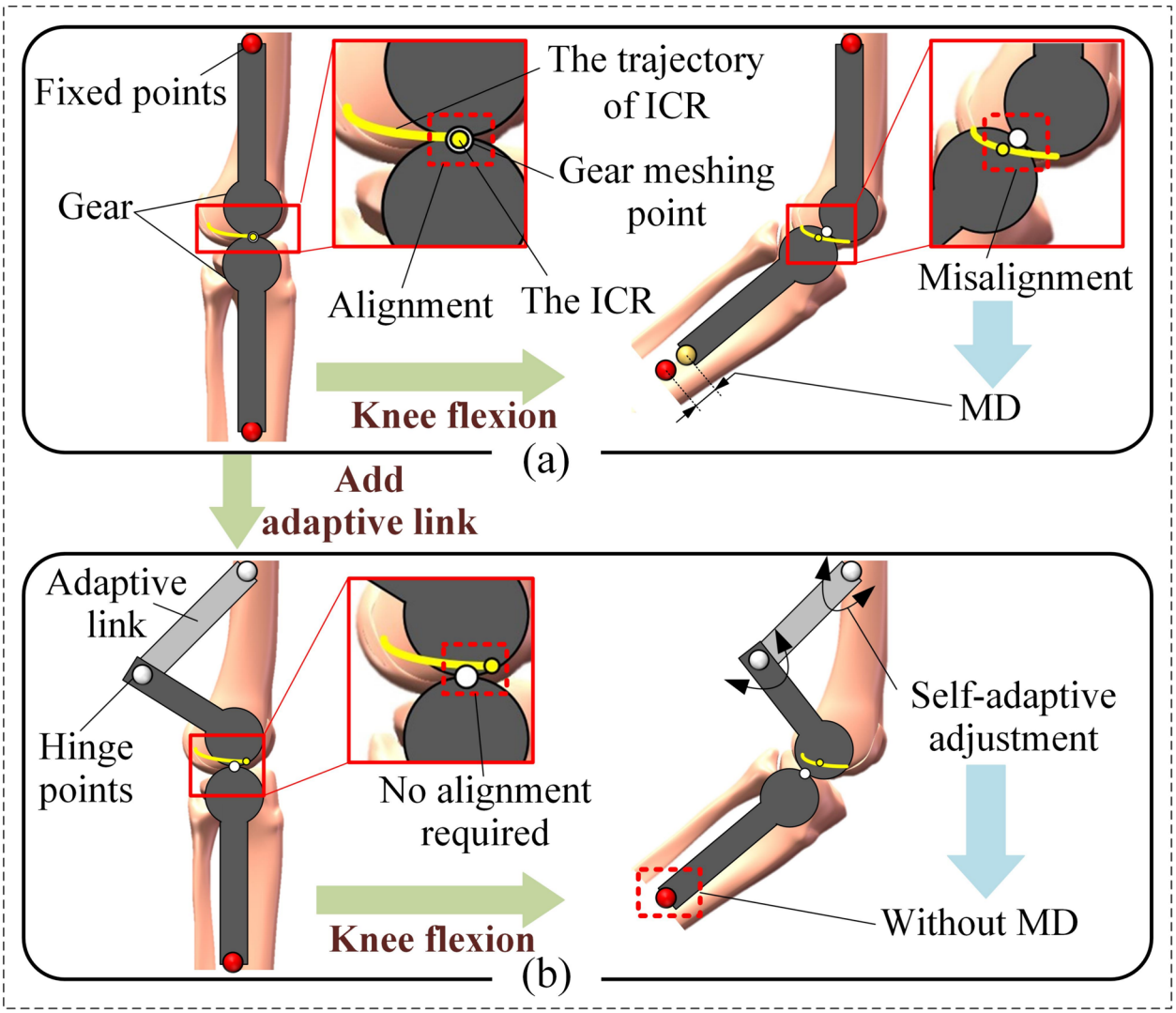

Figure 1 Design concept: **a** Design of biomimetic structures based on gears, **b** Adaptive structural design concept

(2) Gears no longer need to imitate the shape of the human knee joint for design, and their function is also transformed into reducing the DOF of the mechanism.

(3) The exoskeleton can wear multiple positions at the human knee joint.

2.3 Adaptive Knee Exoskeleton Design Based on GLM

According to the concept of adaptive structural design, there are two ways of MD absorption: active and passive. Active absorption means that the two DOFs of absorbing MD are driven, i.e., driving the adaptive link. The driving functions of the adaptive link are determined based on the motion of the human knee joint, with the goal of actively adjusting the exoskeleton posture to absorb the MD caused by misalignment. The advantage of this design approach is that it can provide the auxiliary force required for the assisted limb without generating undesired forces/ moments in human-machine interaction positions. However, actively adapting exoskeletons increases the system's quality and the difficulty of control.

Passive absorption means that the human femur, tibia, knee joint, and exoskeleton mechanism together form a closed-loop chain, constituting a GLM, where the number of DOFs of the GLM is 1. This means that only one active DOF is needed out of three DOFs in the exoskeleton mechanism to assist the motion of the knee joint, while the other two DOFs are passive DOFs to absorb the MD. This passive absorption of MD changes the number of active DOF to one, which is conducive to the lightweight and simplicity of control of the exoskeleton

system. However, it requires the binding position of the exoskeleton to the human body to be secure enough, because the binding position of the exoskeleton to the human body needs to provide the force/moment for the adaptive link to absorb the MD.

Based on the considerations of lightweight and control simplicity of the exoskeleton system, this paper chooses the passive absorption of MD to design an adaptive knee exoskeleton based on GLM, as shown in Figure 2. The drive of the exoskeleton is located in the drive box at the waist, and torque is transmitted to pulley 1 through the Bowden cable. Pulley 1' and pulley 1 move coaxially and synchronously, and torque is ultimately transmitted from pulley 1' to L_3 through pulley 2 and pulley 3 to assist in human knee joint movement. The winding method of the drive cable is shown in Figure 2b.

As shown in Figure 2c, in the GLM, assuming that the femur is fixed during knee joint flexion, the virtual link L_5 of the femur is the frame link of the GLM, L_1 is the adaptive link, and L_5 is hinged with L_1 and L_4; L_2 is hinged with L_1, and L_2 is fixedly connected to gear M at the same time; L_3 is hinged with L_2 and L_6; L_6 is fixedly connected to gear N, and L_6 is fixedly connected to the calf through leg binding; L_4 is a virtual link that comes out of the tibia and is hinged to L_5 while also being hinged to L_3. The hinge point of L_5 and L_4 is the ICR of the knee joint.

During the process of knee joint movement assisted by exoskeletons, virtual link L_5 will change its length accordingly according to the movement of the ICR, while virtual link L_4 will maintain its original length and rotate around and follow the ICR. At the same time, GLM absorbs MD through the adaptive link L_1 in the mechanism, thereby maintaining the binding position of the exoskeleton on the human body.

The WA in Figure 2c is the expected area delineated by us on the exoskeleton device, with a size range set at 40 mm×200 mm. When wearing, the ICR aligns with this area, the angle of exoskeleton assistance should reach at least 120°, and the GLM does not have any singularities during the assistance. The WA extends the "point alignment point" of the rotation axis of the human-machine joints in the sagittal plane to the "face alignment point", which also means that the exoskeleton can be worn in multiple positions on the human body, allowing for faster wear.

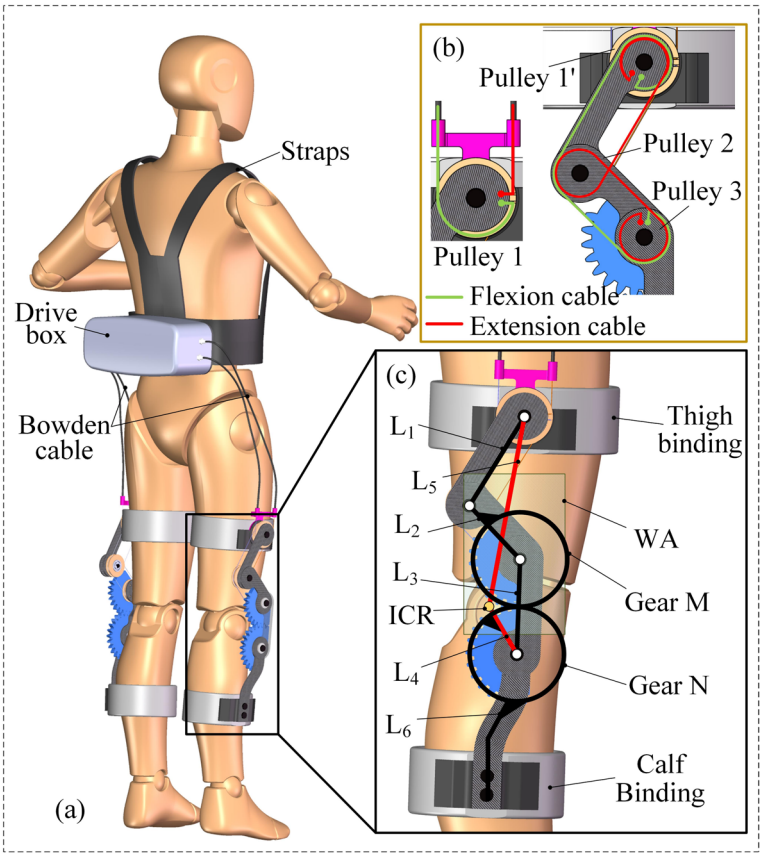

Figure 2 Knee exoskeleton based on GLM: **a** Wearing diagram, **b** driving path, **c** The GLM

We adopted the model proposed by Walker et al. [34] to address the issue of ICR changing with the knee flexion angle. This model describes the average ICR variation of the knee joint flexion angle in the range of 0°~120°, and the trajectory curve described is a function of the knee joint flexion angle. This model has been used as a reference for optimization, simulation, and evaluation in some knee exoskeletons, such as Refs. [20, 22, 35]. In this paper, the trajectory of ICR measured and described by Walker et al. was adjusted to match the coordinate reference system used in this paper, as shown in Figure 3. The origin of the coordinate system is fixed on the femur and coincides with the ICR of the knee joint in the initial state. In this paper, the proposed exoskeleton is analyzed, optimized, and simulated using the trajectory of the adjusted ICR of the knee joint.

3 Kinematic Analysis

3.1 Position Analysis of the GLM

The kinematic model of the GLM is shown in Figure 4. The origin of the world coordinate system is established at point O, with the x-axis and y-axis directions as shown in Figure 4, and the clockwise direction as the positive direction. The lengths of ***OA***, ***AM***, ***MN***, ***NK***, ***OK***, and ***NF*** are l_i ($i=1,\ldots, 6$), respectively. θ_1 is the angle between vector ***OA*** and the positive direction of the x-axis; θ_2 is the angle between vector ***OA*** and vector ***AM***; θ_3 is the angle between vector ***AM*** and vector ***MN***, and is the input angle; θ_4 is the angle between vector ***MN*** and vector ***NK***; θ_K is the angle between ***KN*** and the positive direction of the x-axis; $\Delta\theta_K$ represents the angle of knee joint flexion.

Based on geometric relationships, we can obtain:

$$\theta_K = \theta_1 + \theta_2 + \theta_3 + \theta_4 - \pi. \tag{1}$$

The coordinates of point A, point M, and point N in the world coordinate system can be calculated as:

$$\begin{cases} \boldsymbol{p}_A = \begin{bmatrix} x_A \\ y_A \end{bmatrix} = \begin{bmatrix} l_1 \cos\theta_1 \\ l_1 \sin\theta_1 \end{bmatrix}, \\ \boldsymbol{p}_M = \begin{bmatrix} x_M \\ y_M \end{bmatrix} = \begin{bmatrix} x_A + l_2 \cos(\theta_1 + \theta_2) \\ y_A + l_2 \sin(\theta_1 + \theta_2) \end{bmatrix}, \\ \boldsymbol{p}_N = \begin{bmatrix} x_N \\ y_N \end{bmatrix} = \begin{bmatrix} x_M + l_3 \cos(\theta_1 + \theta_2 + \theta_3) \\ y_M + l_3 \sin(\theta_1 + \theta_2 + \theta_3) \end{bmatrix}. \end{cases} \tag{2}$$

To represent the initial state of the human-machine system more conveniently and distinguish between the initial state and the knee joint flexion state, let α_j be the angle at the initial state of θ_j ($j=1, 2, 3, 4, K$).

In this mechanism, l_1, l_2, l_3, l_6 and α_1, α_2 are known design parameters and define the angle relationship of the initial position:

$$\alpha_1 + \alpha_2 + \alpha_3 = \pi/2. \tag{3}$$

At the initial position, the length of l_4 can be calculated if the position of the ICR of the knee $\boldsymbol{p}_K(x_K, y_K)$ in the world coordinate system is known:

$$l_4 = \sqrt{(x_K - x_N)^2 + (y_K - y_N)^2}. \tag{4}$$

According to the model of Walker et al. [34], the position of the ICR of the knee joint as a function of the flexion angle $\Delta\theta_K$. We can obtain:

$$\begin{cases} x_K = \boldsymbol{g}_x(\Delta\theta_K), \\ y_K = \boldsymbol{g}_y(\Delta\theta_K), \end{cases} \tag{5}$$

where $\boldsymbol{g}$ is the mapping function from the knee joint flexion angle to the position of the ICR.

Establish the closed-loop vector equation:

$$\boldsymbol{OA} + \boldsymbol{AM} + \boldsymbol{MN} + \boldsymbol{NK} = \boldsymbol{OK}. \tag{6}$$

Rewritten as a projection equation:

$$\begin{cases} x_N + l_4 \cos(\theta_1 + \theta_2 + \theta_3 + \theta_4) = x_K, \\ y_N + l_4 \sin(\theta_1 + \theta_2 + \theta_3 + \theta_4) = y_K. \end{cases} \tag{7}$$

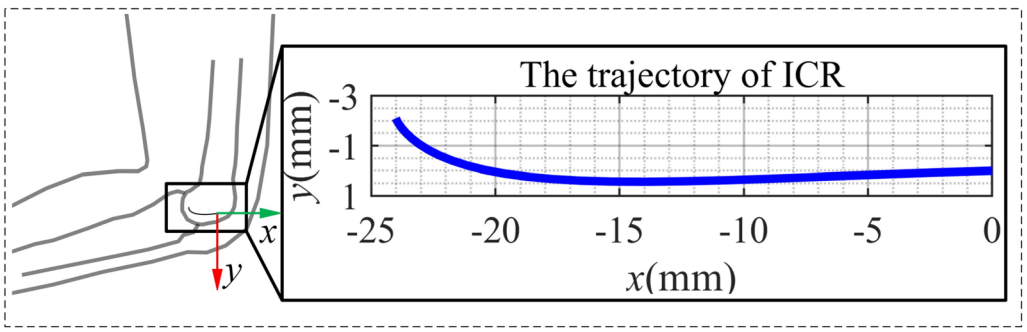

Figure 3 The trajectory of ICR of the knee joint

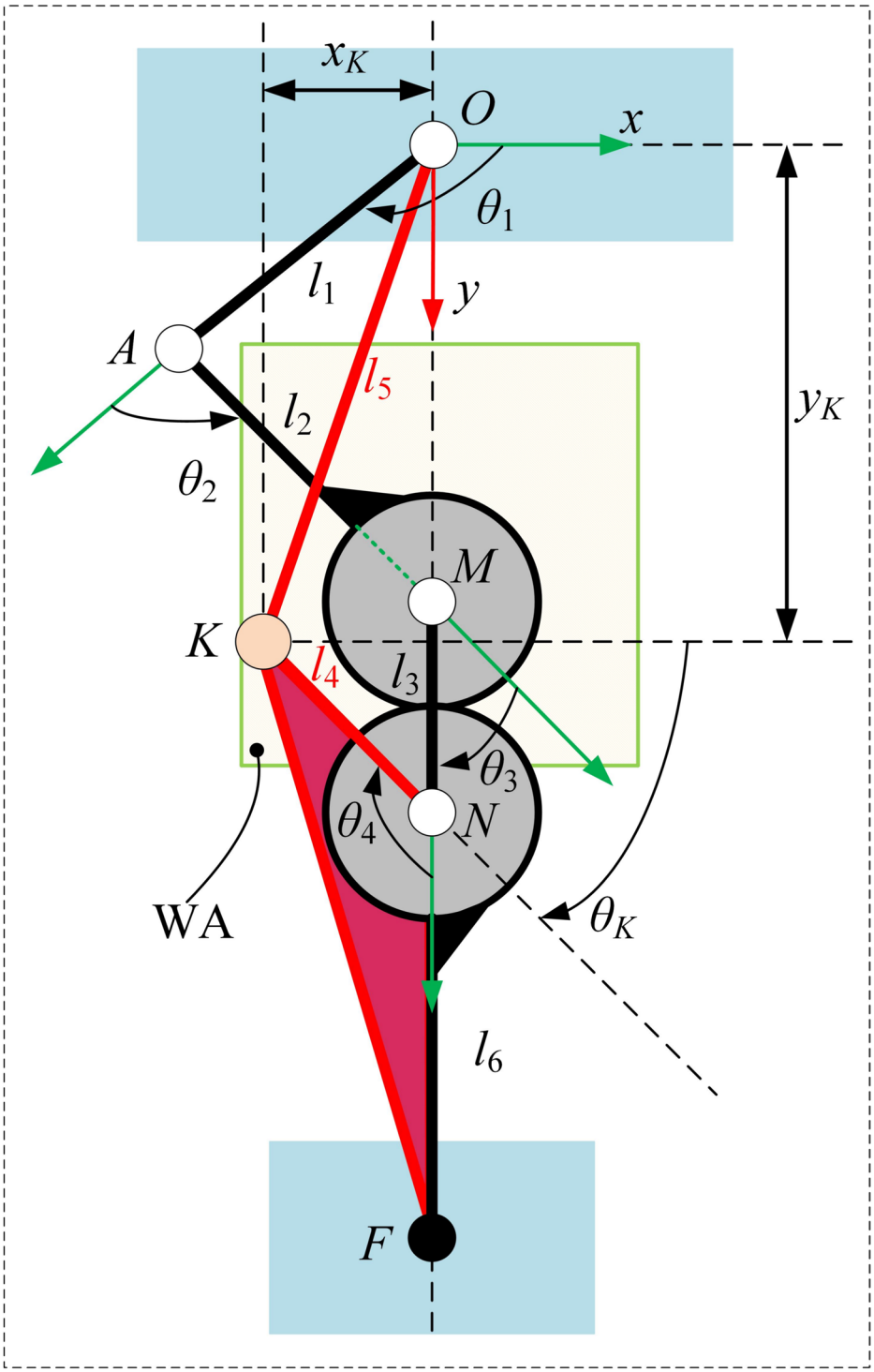

Figure 4 The kinematic model of the GLM

The relationship between θ_3 and θ_4 is:

$$\theta_3 - \alpha_3 = n(\theta_4 - \alpha_4). \tag{8}$$

Eqs. (7) and (8) are the constraint equations for the GLM. Among them, θ_3 is the known input angle; n is the transmission ratio of the gears.

The size parameters of the GLM are shown in Table 1. The position line diagrams are shown in Figure 5.

3.2 Velocity Analysis of GLM

In the analysis of the velocity of the mechanism, we also considered the velocity of the movement of the ICR of the knee joint. Eqs. (1), (7), and (8) are obtained by derivation for time:

$$\begin{cases} a_{11}\dot{\theta}_1 + a_{12}\dot{\theta}_2 + a_{13}\dot{\theta}_3 + a_{14}\dot{\theta}_4 = \dot{x}_K, \\ a_{21}\dot{\theta}_1 + a_{22}\dot{\theta}_2 + a_{23}\dot{\theta}_3 + a_{24}\dot{\theta}_4 = \dot{y}_K, \\ \dot{\theta}_3 - n\dot{\theta}_4 = 0, \\ \dot{\theta}_1 + \dot{\theta}_2 + \dot{\theta}_3 + \dot{\theta}_4 - \dot{\theta}_K = 0, \end{cases} \tag{9}$$

where $a_{11}=l_1s_1+l_2s_{12}+l_3s_{123}+l_4s_{1234}$, $a_{12}=l_2s_{12}+l_3s_{123}+l_4s_{1234}$, $a_{13}=l_3s_{123}+l_4s_{1234}$, $a_{14}=l_4s_{1234}$, $a_{21}=l_1c_1+l_2c_{12}+l_3c_{123}+l_4c_{1234}$, $a_{22}=l_2c_{12}+l_3c_{123}+l_4c_{1234}$, $a_{23}=l_3c_{123}+l_4c_{1234}$, $a_{24}=l_4c_{1234}$, s_1 denotes $\sin\theta_1$, s_{12} denotes $\sin(\theta_1+\theta_2)$, c_1 denotes $\cos\theta_1$, c_{12} denotes $\cos(\theta_1+\theta_2)$, and:

$$\begin{cases} \dot{x}_K = G_x\left(\dot{\theta}_1 + \dot{\theta}_2 + \dot{\theta}_3 + \dot{\theta}_4\right), \\ \dot{y}_K = G_y\left(\dot{\theta}_1 + \dot{\theta}_2 + \dot{\theta}_3 + \dot{\theta}_4\right), \end{cases} \tag{10}$$

where $G_x = \frac{\partial \boldsymbol{g}_x(\Delta\theta_K)}{\partial(\Delta\theta_K)}$, $G_y = \frac{\partial \boldsymbol{g}_y(\Delta\theta_K)}{\partial(\Delta\theta_K)}$.

Decompose Eq. (10) into active and passive parts as follows:

$$\boldsymbol{J}_p\dot{\boldsymbol{q}}_p + \boldsymbol{J}_a\dot{\theta}_3 = 0, \tag{11}$$

where $\boldsymbol{J}_a$ is the part corresponding to the active joints, $\boldsymbol{J}_p$ is the part corresponding to the passive joints, and $\boldsymbol{q}_p$ is the passive joint motion parameters. And:

$$\begin{cases} \boldsymbol{J}_a = \begin{bmatrix} a_{13} + G_x & a_{23} - G_y & 1 & 1 \end{bmatrix}^{\mathrm{T}}, \\ \boldsymbol{J}_p = \begin{bmatrix} a_{11} + G_x & a_{12} + G_x & a_{14} + G_x & 0 \\ a_{21} - G_y & a_{22} - G_y & a_{24} - G_y & 0 \\ 0 & 0 & -n & 0 \\ 1 & 1 & 1 & -1 \end{bmatrix}, \\ \dot{\boldsymbol{q}}_p = \begin{bmatrix} \dot{\theta}_1 & \dot{\theta}_2 & \dot{\theta}_4 & \dot{\theta}_K \end{bmatrix}^{\mathrm{T}}. \end{cases}$$

Thus, the relationship between the active and passive joints is:

$$\dot{\boldsymbol{q}}_p = \boldsymbol{J}\dot{\theta}_3, \tag{12}$$

where the Jacobi matrix $\boldsymbol{J}=-\boldsymbol{J}_p^{-1}\boldsymbol{J}_a$ is the velocity mapping from the active joint to the passive joints. Let the angular velocity of the active joint be 30°/s, then the velocity mapping line diagram from the active joint to the passive joints is shown in Figure 6.

3.3 Validation of the Kinematic Model

The subsequent performance analysis and sizing optimization of the GLM is based on the kinematic model, so the correctness of the kinematic model is crucial. Here, we use Adams-MATLAB co-simulation to verify the correctness of the kinematic model. As shown in Figure 7(a), the trajectory of ICR is given in the human-machine physical system established in Adams. Figure 7b illustrates the interactive computation process between Adams and MATLAB. Initially, Adams transmits the measured knee flexion angle $\Delta\theta_K$ to MATLAB for the mathematical model. Subsequently, the mathematical model computes the changes Δx and Δy in the knee joint's center of rotation based on the knee flexion angle $\Delta\theta_K$. This information, along with the initial position of the ICR (x_{K0}, y_{K0}), is used to determine the current position of the knee ICR (x_K, y_K), which is then transmitted to the human-machine physical system within Adams. The simulation is set to last for 2 seconds, during which the angle and angular velocity of each joint in the GLM are output in Adams.

The comparison of the theoretical values of angles and angular velocities of each joint in the GLM with the simulated values of the Adams-MATLAB co-simulation is shown in Figure 8. The curves of the theoretical and simulated values of the angles and angular velocities of the joints in the GLM in Figure 8 basically match, thus verifying the correctness of the kinematic model.

Table 1 The size parameters of the exoskeleton mechanism

Parameters	Values
l_1 (mm)	110
l_2 (mm)	77.6
l_3 (mm)	100
α_1 (°)	120
α_2 (°)	−75.14
n	−1
$\boldsymbol{P}_K$ (mm)	(−10, 160)

4 Performance Analysis

4.1 Size of the WA

The size of the WA reflects the convenience of aligning the rotation axis of the human-machine joint when wearing the exoskeleton. The larger the WA, the more

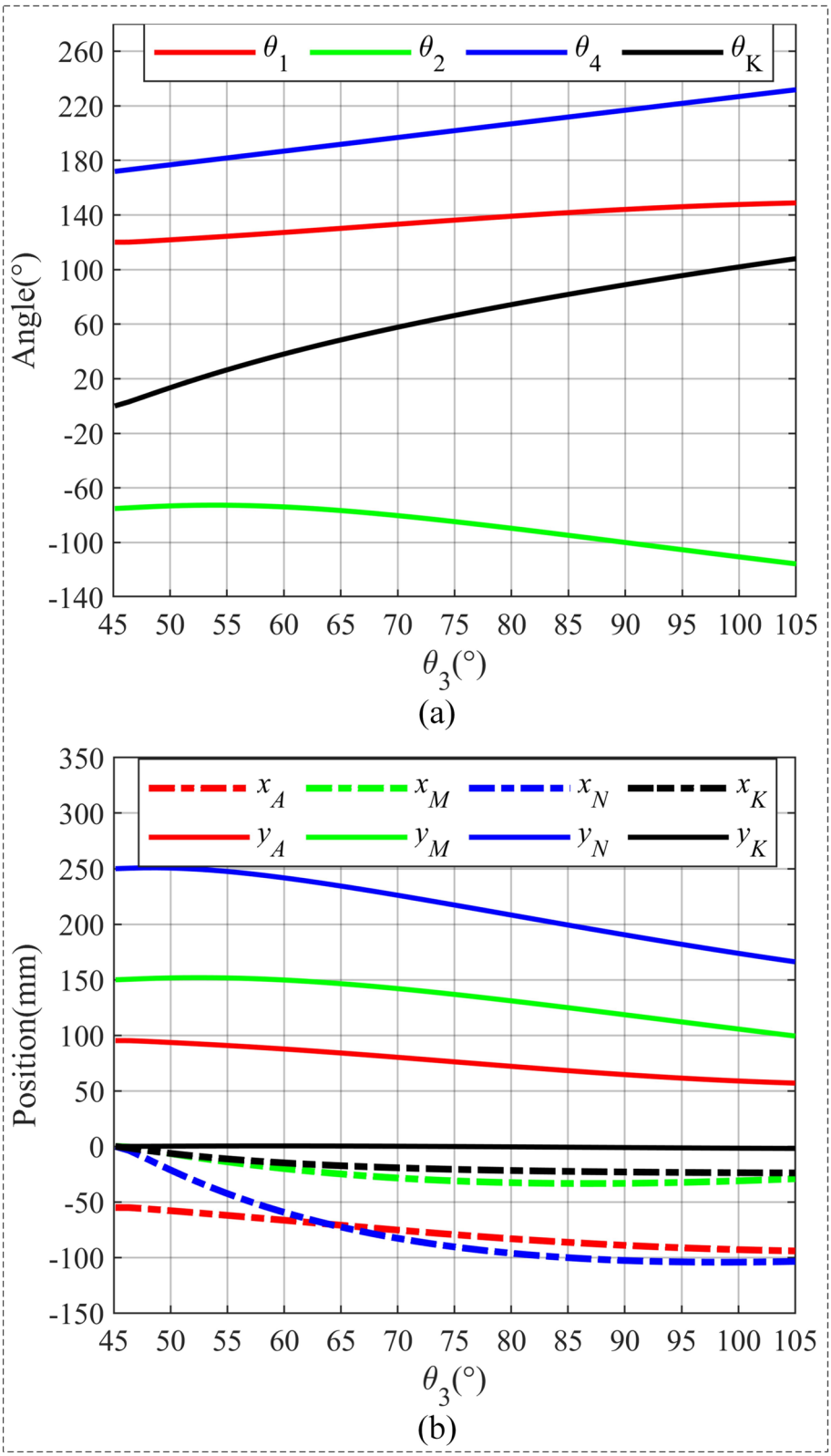

Figure 5 Kinematic curves under initial exoskeleton parameters: **a** Angle line diagram, **b** Position line diagram

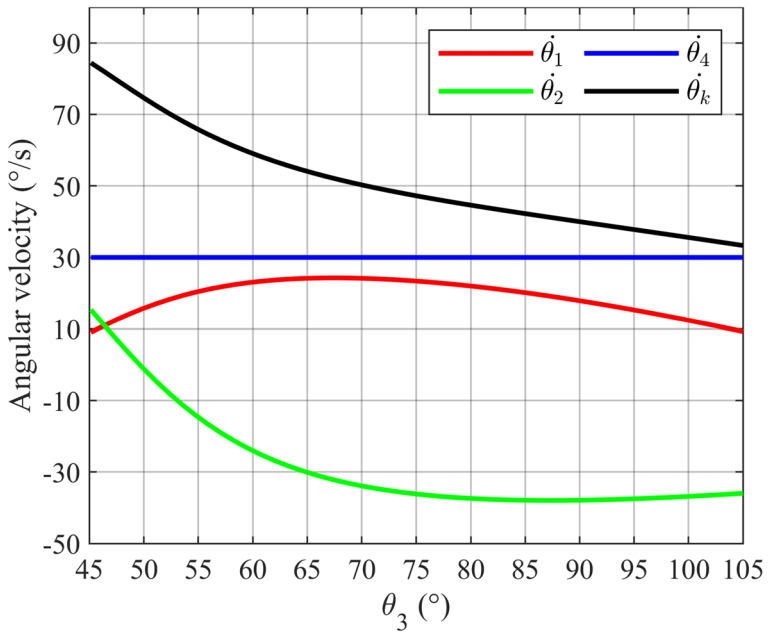

Figure 6 Passive joints angular velocity line diagram

convenient it is for the alignment of the rotation axis of the human-machine joints when wearing the exoskeleton.

In this paper, the exoskeleton mechanism and the human femur, tibia, and knee joint together form a 1-DOF GLM. During its movement, singular configurations may occur, resulting in the mechanism not being able to assist human motion normally. Therefore, in the design process, it is necessary to avoid these singular configurations. According to the input and output velocity relationship of the closed-loop mechanism, singular configurations can be divided into three categories: forward kinematic singularity, inverse kinematic singularity, and combined singularity.

(1) Forward kinematics singularity (input singularity), matrix $\boldsymbol{J}_p$ rank reduction. $\boldsymbol{J}_p$ represents the passive joints Jacobian matrix, and when $\boldsymbol{J}_p$ is reduced in rank, the output variable of the active joint variable cannot be represented.

When the mechanism is located in this singular position, after fixing the active joint, the passive joints of the mechanism still have instantaneous motion. At this point, $\det(\boldsymbol{J}_p)=0$, which satisfies:

$$l_1 n\left(G_x c_1 + G_y s_1 + l_2 s_2 + l_3 s_{23} + l_4 s_{234}\right) = 0. \quad (13)$$

(2) Inverse kinematic singularity (output singularity), matrix $\boldsymbol{J}_a$ rank reduction. $\boldsymbol{J}_a$ represents the Jacobian matrix of the active joint. When the mechanism is in this singular position and the active joint has output, the passive joints of the mechanism do not have output motion. At this point, it is necessary to ensure that every element in $\boldsymbol{J}_a$ is 0, but it is impossible for every element in $\boldsymbol{J}_a$ to be 0, so the mechanism will not exhibit inverse kinematic singularity.

(3) Combined singularity. This type of singularity is a combination of forward kinematic singularity and inverse kinematic singularity, which simultaneously satisfies the rank reduction of matrix $\boldsymbol{J}_b$ and matrix $\boldsymbol{J}_a$. At this point, when the active joint is locked, the passive joints will still have instantaneous motion, and when the active joint is in motion, the passive joints will not move. The GLM will not experience such singularity.

In summary, the GLM selects θ_3 as the active joint, and forward kinematic singularity may occur, rather than inverse kinematic singularity and combination singularity. Eq. (13) provides a basis for eliminating wearing positions that may exhibit singularity in the WA.

Considering the actual wearing situation of the exoskeleton, we set an expected WA in the world coordinate system: $-20\ \text{mm} < x_K < 20\ \text{mm}$, $50\ \text{mm} < y_K < 250\ \text{mm}$. Set the variation range of the active angle θ_3 to 0°~90°. The WA under the initially selected exoskeleton size parameters is shown in Figure 9. However, under the initially selected exoskeleton size parameters, the WA in Figure 9 does not fill the area we set, there are also some position points that do not meet the wearable requirements, indicating that the initially selected exoskeleton size parameters are not the optimal size parameters.

To characterize the size of the WA (SWA), we use the number of position points *num* to characterize:

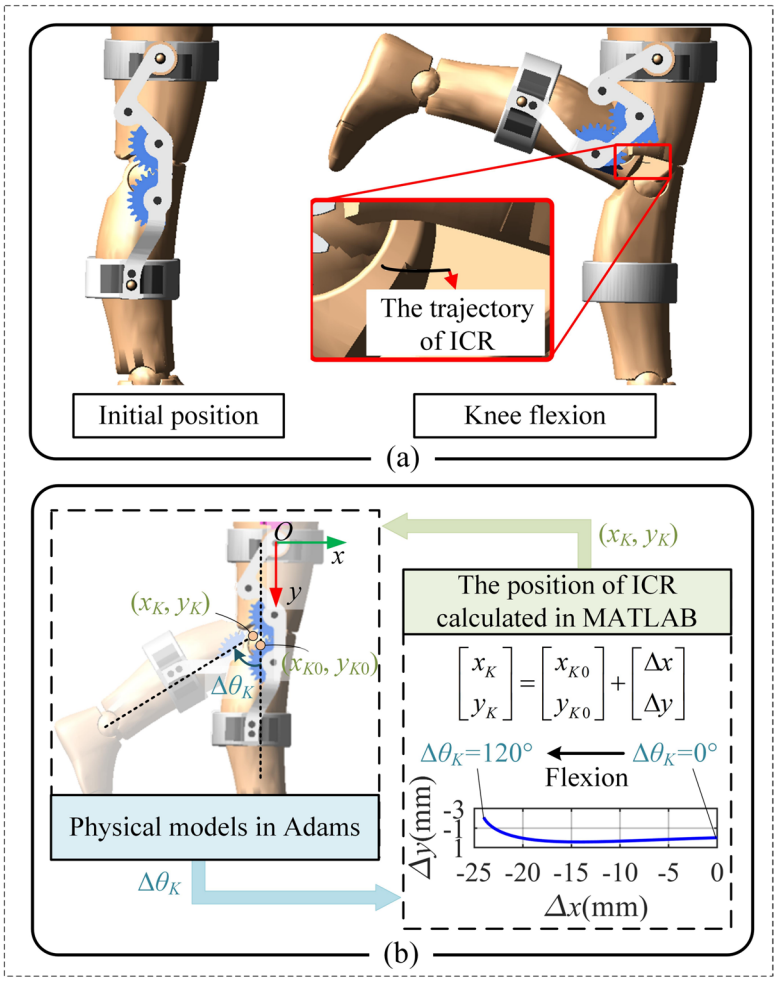

Figure 7 Adams-MATLAB co-simulation: **a** Human-machine physical system built in Adams, **b** Information flow between Adams and MATLAB, $\Delta\theta_K$ is the flexion angle of the knee joint, (x_{K0}, y_{K0}) is the position of the knee joint rotation center in the global coordinate system at the initial position, and (x_K, y_K) is the position of the knee joint rotation center at the current knee joint flexion angle

$$\mathrm{SWA} = num. \tag{14}$$

4.2 Velocity Transfer Ratio

Velocity transfer ratio expresses, as does kinematic manipulability, the ability to transfer velocity from the active joints to the passive output joints. In this paper, the input angle is θ_3 and the output angle of interest is θ_K which is obtained from Eq. (12):

$$\dot{\theta}_K = \gamma\dot{\theta}_3, \tag{15}$$

where γ is a scalar, i.e., a velocity scaling factor from the active joint to the passive output joint. To express the ability to transfer the velocity from the active joint to the knee joint, the local velocity transfer ratio w_v is defined as:

$$w_v = \sqrt{\|\gamma\|}, \tag{16}$$

where w_v denotes the velocity transfer ratio for the specific size parameters, a certain wearing position, and a certain angle of motion. The local velocity transmission ratio in the driving range at the initially selected size parameters is shown in Figure 10a. From this curve, the local velocity transfer ratio decreases with the increase of the flexion angle of the knee joint.

To evaluate the average velocity transfer ratio of an exoskeleton mechanism at a certain wearing position for the specific size parameters, defined:

$$w_{gv} = \frac{\sum_{i=1}^{N} w_{vi}}{N}, \tag{17}$$

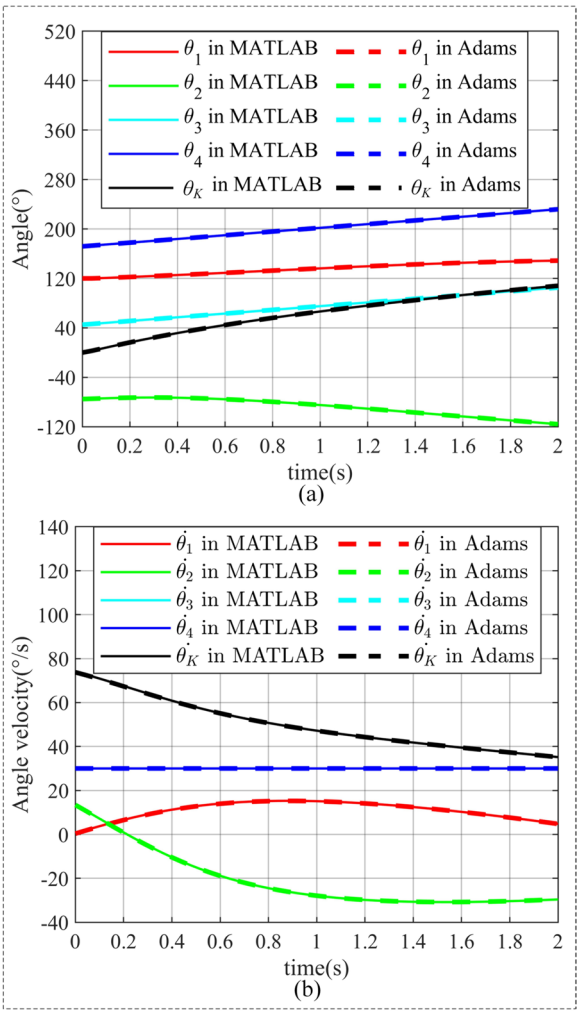

Figure 8 Comparison of theoretical and calculated values: **a** Comparison of angular curves, **b** Comparison of angular velocity curves

where w_{gv} is the average velocity transfer ratio from the active joint to the knee joint during the movement of the knee joint from 0° to 120°; N is the number of selected movement angles; and w_{vi} is the local velocity transfer ratio corresponding to the ith point. The average velocity transfer ratio within the WA under the initially selected exoskeleton size parameters is shown in Figure 10b, where the closer the wearable position is to the origin coordinates of the world coordinate system in the y-axis direction, the larger the average velocity transfer ratio is.

In order to reflect the average transfer ratio of different size parameters in their corresponding WA, the performance index AVTR is defined as:

$$\mathrm{AVTR} = \frac{\sum_{j=1}^{num} w_{gvj}}{num} = \frac{\sum_{j=1}^{num} \left(\sum_{i=1}^{N} w_{vi} \Big/ N \right)_j}{num}, \tag{18}$$

where w_{gvj} is the average velocity transfer ratio corresponding to the jth wearable spatial location at the particular size parameters.

4.3 Initial Position Static Stiffness

Stiffness is the ability to resist deformation under external forces. The stiffness performance of a mechanism is mainly affected by the material and size of the parts as well as the configuration of the mechanism. In the calculation process, let the joints and links in the mechanism be rigid, and let the virtual displacement of the active joint of the mechanism be $\delta\theta_3$, the active joint torque be τ_3, the virtual displacement of the output joint be $\delta\theta_K$, and the output torque be T. According to the principle of virtual work, we have:

$$\tau_3 \delta\theta_3 - T\delta\theta_K = 0. \tag{19}$$

The active joint torque versus output torque is obtained from Eqs. (15) and (19):

$$\tau_3 = \gamma T. \tag{20}$$

Let $\Delta\theta_3$ be the small displacement of the active joint and k be the stiffness coefficient at the active joint, then we have:

$$\tau_3 = k\Delta\theta_3. \tag{21}$$

Associative Eqs. (15), (20) and (21) can be obtained:

$$\Delta\theta_K = \gamma k^{-1} \gamma T. \tag{22}$$

Setting the static stiffness coefficient of the output joints as K_s, it can be obtained:

$$T = K_s \Delta\theta_K. \tag{23}$$

Substituting Eq. (22) into Eq. (23) yields the static stiffness coefficient of the output joint:

$$K_s = k\gamma^{-2}. \tag{24}$$

This static stiffness coefficient characterizes the ability of the exoskeleton mechanism to resist external torque. For a knee exoskeleton mechanism, it is necessary to have a high static stiffness when the knee joint is in the support phase to resist knee flexion and ensure the stability of the human body. Therefore, for the static stiffness analysis, we need to focus on the static stiffness of the GLM when the human limb is in the support phase

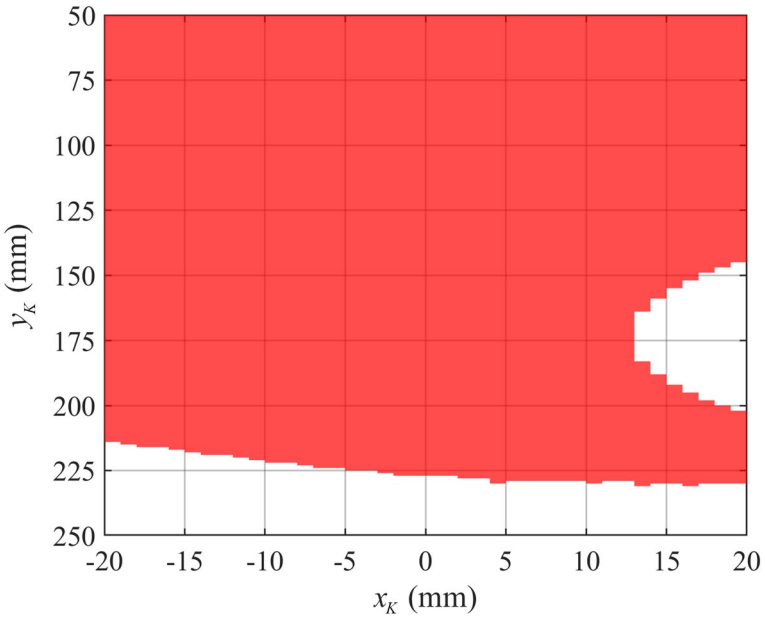

Figure 9 WA under the initially selected exoskeleton size parameters. When wearing, align the center of rotation of the human knee joint with this area, which can ensure that (1) the exoskeleton can assist in the flexion of the human knee joint to 120 °, and (2) no singularity occurs during this process

(initial position). Assuming the stiffness coefficient $k=1$ N/° at the active joint, the initial position static stiffness of the GLM in the WA is shown in Figure 11 while comparing with Figure 10, it can be seen that the initial position static stiffness performs the opposite to the average velocity transfer ratio performance, and the average velocity transfer ratio is instead smaller in the wearable position points with large initial position static stiffness.

To characterize the static stiffness performance of the knee joint in its initial position within the WA under different size parameters, the performance index AISS is defined:

$$\mathrm{AISS}=\frac{\sum_{j=1}^{num} K_{sj}}{num}, \tag{25}$$

where K_{sj} is the initial position static stiffness corresponding to the jth wearing position at the particular size parameters.

5 Optimization

5.1 Formulation of the Optimization Problem

The link lengths of the GLM are the important parameters that affect the performance of the WA, velocity transfer ratio, and initial position static stiffness. In order to obtain a larger WA as well as larger AVTR and AISS, the NSGA-II (Nondominated Sorting Genetic Algorithm II) algorithm is used in this section to optimize the size parameters of the exoskeleton mechanism. This optimization algorithm is a popular classical algorithm among multi-objective evolutionary algorithms, which overcomes the shortcomings of the NSGA algorithm that does not retain the optimal individuals during iteration, the shared parameter values are difficult to determine, and the time complexity of the construction of the Pareto optimal solution set is high, with fast computation speed and high efficiency, and it has a unique advantage for the complex and large-scale optimization problems [36, 37].

Establish the multi-parameter multi-objective problem as:

$$\begin{cases} \min & f_{\mathrm{m}}(\boldsymbol{x})(m=1,\ldots,3), \\ \text{s.t.} & \boldsymbol{x}\in C, \end{cases} \tag{26}$$

where $\boldsymbol{x}\in[l_1,l_2,l_3,\alpha_1,\alpha_2]$ is the selected size optimization parameters of the GLM; $f_m(\boldsymbol{x})$ ($m=1$, 2, 3) are the defined objective functions, and $f_1(\boldsymbol{x})=-\mathrm{SWA}$, $f_2(\boldsymbol{x})=-\mathrm{AVTR}$, and $f_3(\boldsymbol{x})=-\mathrm{AISS}$; and C is the constraints of the five optimization parameters during the size optimization process of the mechanism, the upper and lower bounds of which are shown in Table 2. In this paper, the gear ratio $n=-1$ is not used as an optimization parameter because the role of the gears in our design is only to reduce the DOF of the mechanism to 1. In order to ensure that the exoskeleton mechanism has a sufficient WA, the constraint $\mathrm{SWA}>2000$ is used in the optimization process.

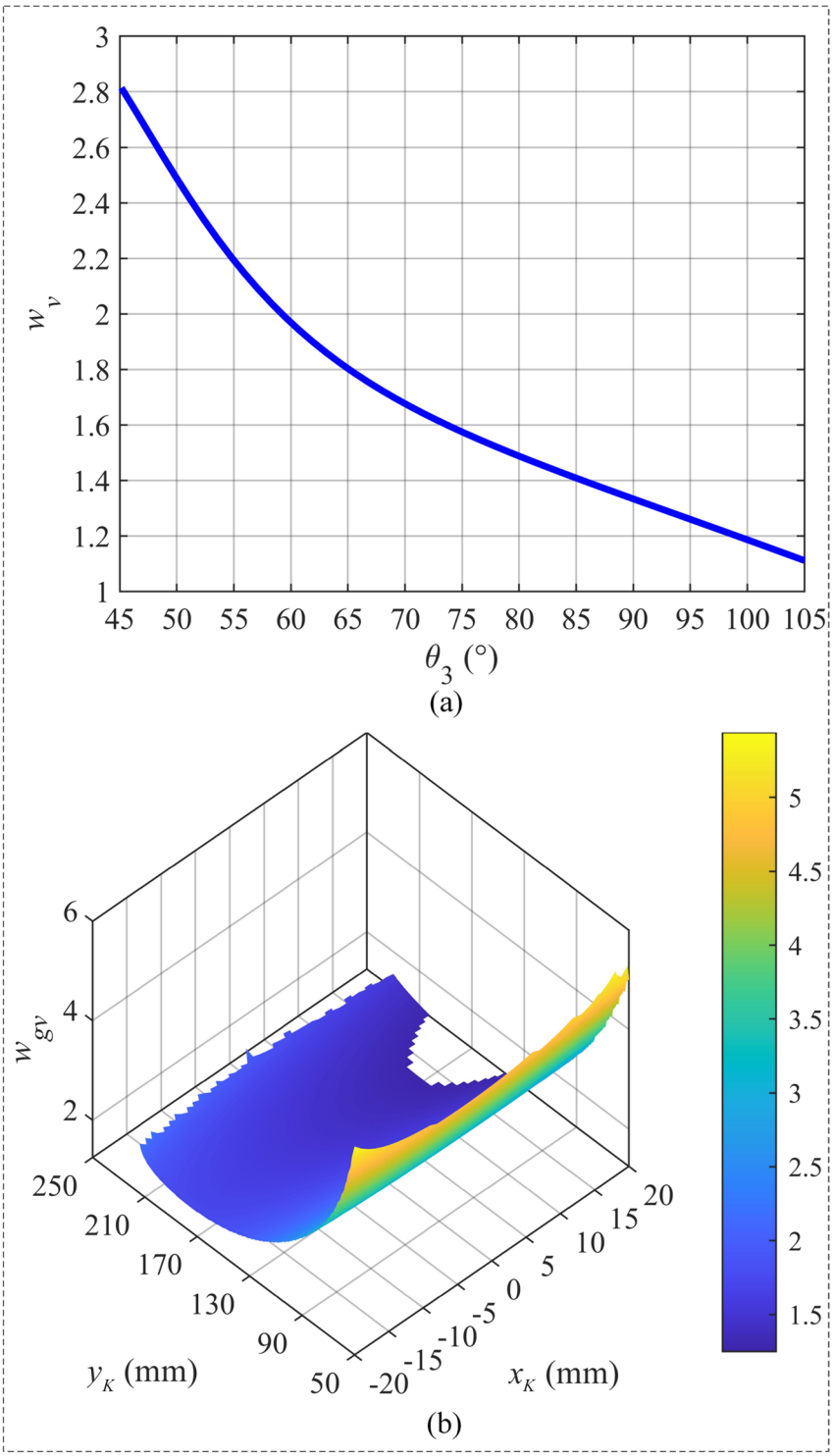

Figure 10 Velocity transfer ratio: **a** The velocity transfer ratios at a particular wearing position for the given size parameters, **b** The average velocity transfer ratios within the WA for the given size parameters

5.2 Optimization Results

In the NSGA-II optimization algorithm, the population size is set to 60, the number of generations is 120, the crossover probability is 0.9, and the mutation probability is 0.05. The Pareto frontiers of the objective functions f_1, f_2, and f_3 and their trends with the number of generations

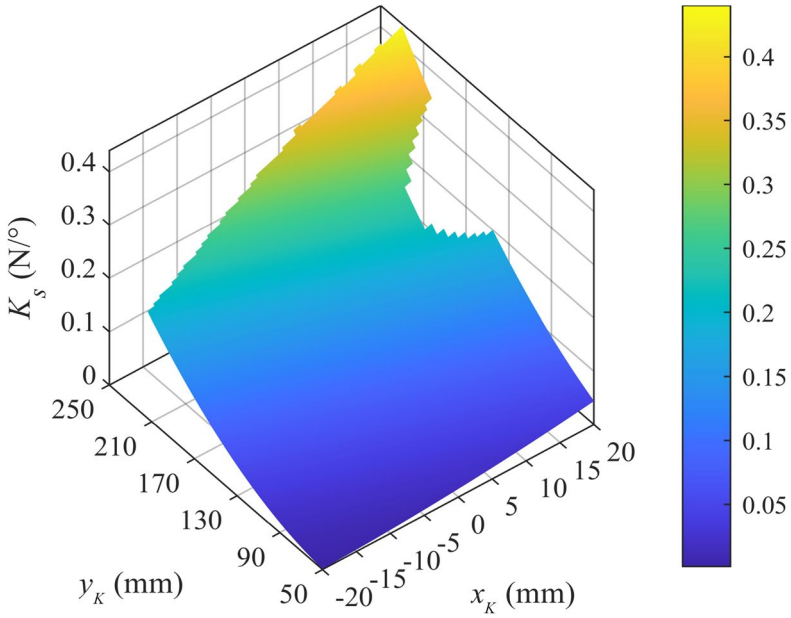

Figure 11 Static stiffness at the initial position within the WA

Table 2 Bounds of the parameters

Parameters	Bounds
l_1 (mm)	(70, 120)
l_2 (mm)	(70, 120)
l_3 (mm)	(70, 120)
a_1 (°)	(90, 180)
a_2 (°)	(−180, 0)

of heredity after the optimization are shown in Figure 12, and the SWA has been stabilized at around the 80th generation.

The final optimization yields 60 sets of size parameters, and the optimal solution needs to be selected among these 60 sets of size parameters. Since the three optimization objectives have different scales, we need to define a comprehensive performance indicator (CPI):

$$\mathrm{CPI} = \omega_1 \frac{num}{\frac{1}{pop}\sum_{M=1}^{pop} num} + \omega_2 \frac{\mathrm{AVTR}}{\frac{1}{pop}\sum_{M=1}^{pop} \mathrm{AVTR}} + \omega_3 \frac{\mathrm{AISS}}{\frac{1}{pop}\sum_{M=1}^{pop} \mathrm{AISS}}, \tag{27}$$

where ω is the weight coefficient, we pay more attention to the SWA, so we set $\omega_1 = 0.6$, $\omega_2 = 0.2$, $\omega_3 = 0.2$. And $pop = 60$ is the population size.

The set of size parameters with the largest CPI value is taken, and the optimized size parameters are obtained as shown in Table 3.

5.3 Performance Comparison Before and After Optimization

The comparison before and after the optimization of the three indicators is shown in Figure 13. After optimizing the size parameters, the SWA increased by 18.40% as shown in Table 4, and the set areas are all wearable. Also, the AVTR on the WA increased by 4.98% and the AISS increased by 6.01%. This means that the exoskeleton mechanism has a larger WA on the human body and better performs on the larger WA.

6 Simulation and Compatibility Test

In this section, the ability of the exoskeleton mechanism to absorb MD is verified through Adams-MATLAB co-simulation. And the compatibility of human-machine kinematics was verified through a mechanism principle prototype.

6.1 Simulation of MD Absorption

To simulate the absorption of undesired MD by the proposed exoskeleton during assisted human knee motion, we set the human knee flexion motion as the active motion in the simulation environment. Additionally, we set the knee flexion angular velocity to 45°/s, and a constant assisted torque of 10 Nm is given to the active joint θ_3 of the exoskeleton. It is assumed that the human-machine interaction positions have an equivalent stiffness coefficient of 1 N/mm and an equivalent damping coefficient of 1 N·mm/s, after being strapped to the human body. The change of the MD, the change of the

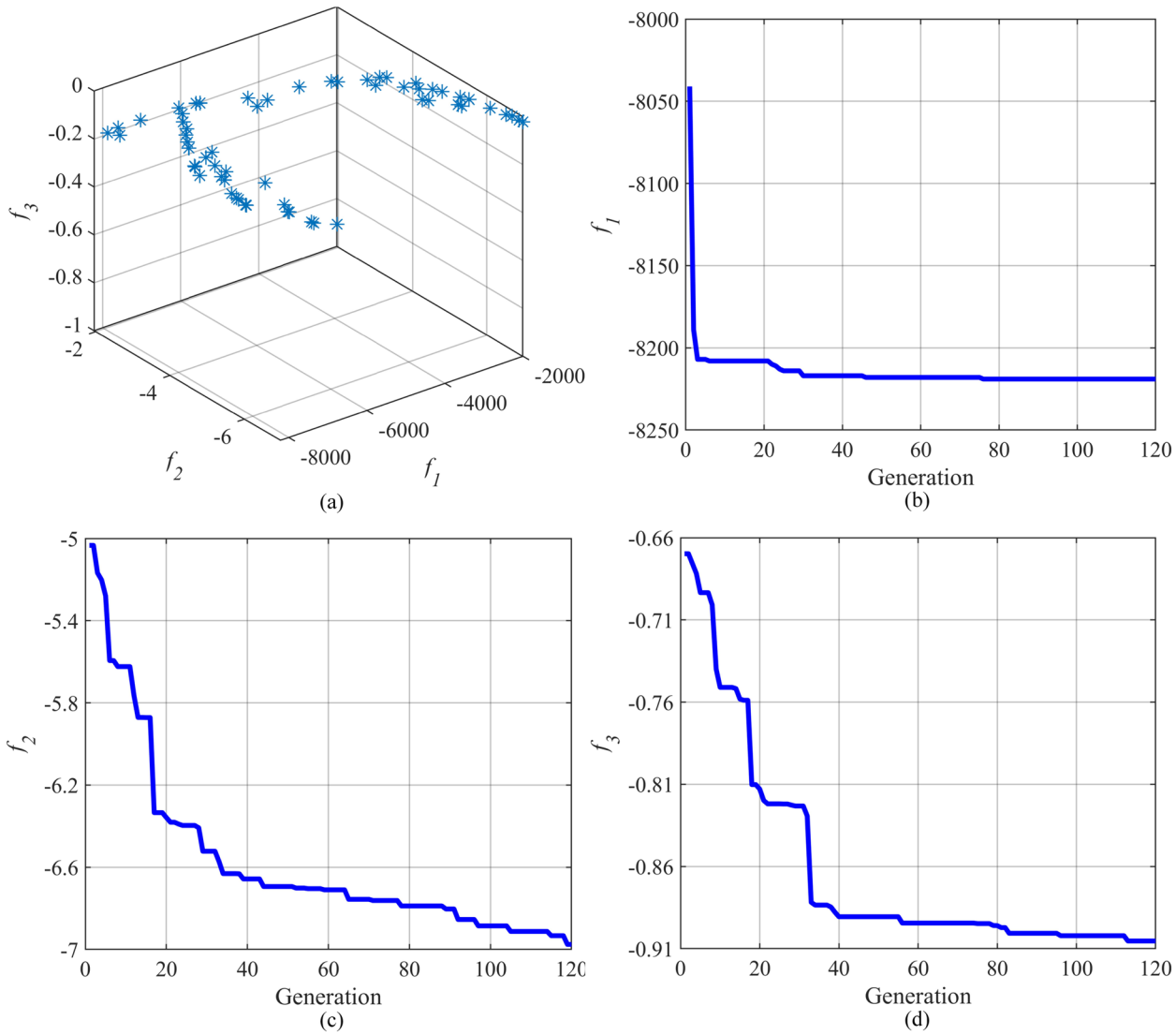

Figure 12 Optimization results: **a** Pareto front, **b** Trend of the WA with genetic generations, **c** Trend of AVTR with genetic generations in the WA, **d** Trend of AISS with genetic generations in the WA

Table 3 Optimized size parameters

Parameters	Values
l_1 (mm)	120
l_2 (mm)	98.88
l_3 (mm)	74.17
a_1 (°)	114.71
a_2 (°)	− 49.25

adaptation angles $\Delta\theta_1$ and $\Delta\theta_2$ (clockwise direction as the positive direction), and the force along the leg surface F_{calf} and F_{thigh} (down along the leg surface as the positive direction) are measured in the assisting process, and the simulation time is 2 s.

Simulation a: Simulation of the generation of MD in a gear-like exoskeleton. The two adaptive angles $\Delta\theta_1$ and $\Delta\theta_2$ of the adaptive link are fixed, i.e., the exoskeleton is made to lose its adaptive ability. Due to the misalignment of the center of rotation of the knee joint and the gear meshing point, there is bound to be the MD generation at the interaction positions between the exoskeleton and the human body. As shown in Figure 14a, the MD_{calf} and MD_{thigh} of the exoskeleton on the calf and thigh, as well as the force F_{calf} and F_{thigh} of the exoskeleton on the calf and thigh are measured. The

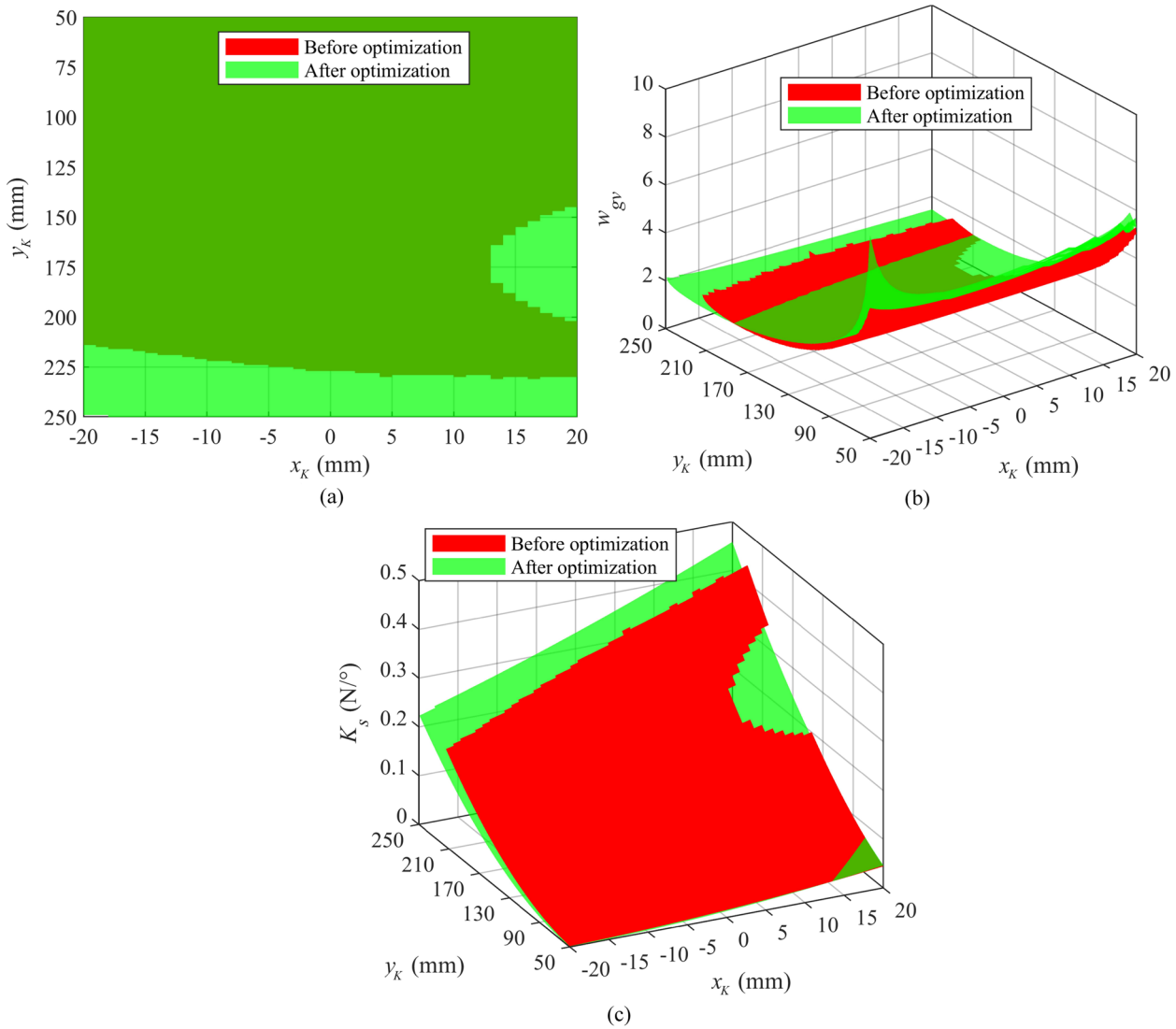

Figure 13 Comparison of performance before and after optimization: **a** Comparison of SWA, **b** Comparison of AVTR within the WA, **c** Comparison of AISS within the WA

Table 4 Performance before and after optimization

Performance parameters	Before optimization	After optimization	Performance improvement percentage (%)
SWA	6941	8218	18.40
AVTR	2.21	2.32	4.98
AISS	0.133	0.141	6.01

peak of the MD_{calf} can reach up to 40 mm, the peak of the MD_{thigh} can be up to 19 mm, the peak of the F_{calf} can be up to 65 N, and the peak of the F_{thigh} can be up to 30 N.

Simulation b: Activating the adaptive link. As shown in Figure 14b, after activating the adaptive link, the MD in Figure 14a can be transformed into the changing angle of the adaptive link, which is absorbed by the exoskeleton mechanism. At this time, the peak of MD_{calf} decreased to 2.3 mm, the peak of MD_{thigh} decreased to 1.4 mm, the peak of F_{calf} decreased to 7 N, and the peak of F_{thigh} decreased to 3 N.

Simulation c: Activating the adaptive link. The sliding displacement (SD) of the exoskeleton along the leg surface is arbitrarily given as $s=20\sin(\pi t/4)$ mm to verify the adaptive ability of the exoskeleton when a sliding situation occurs during the assisting process. As

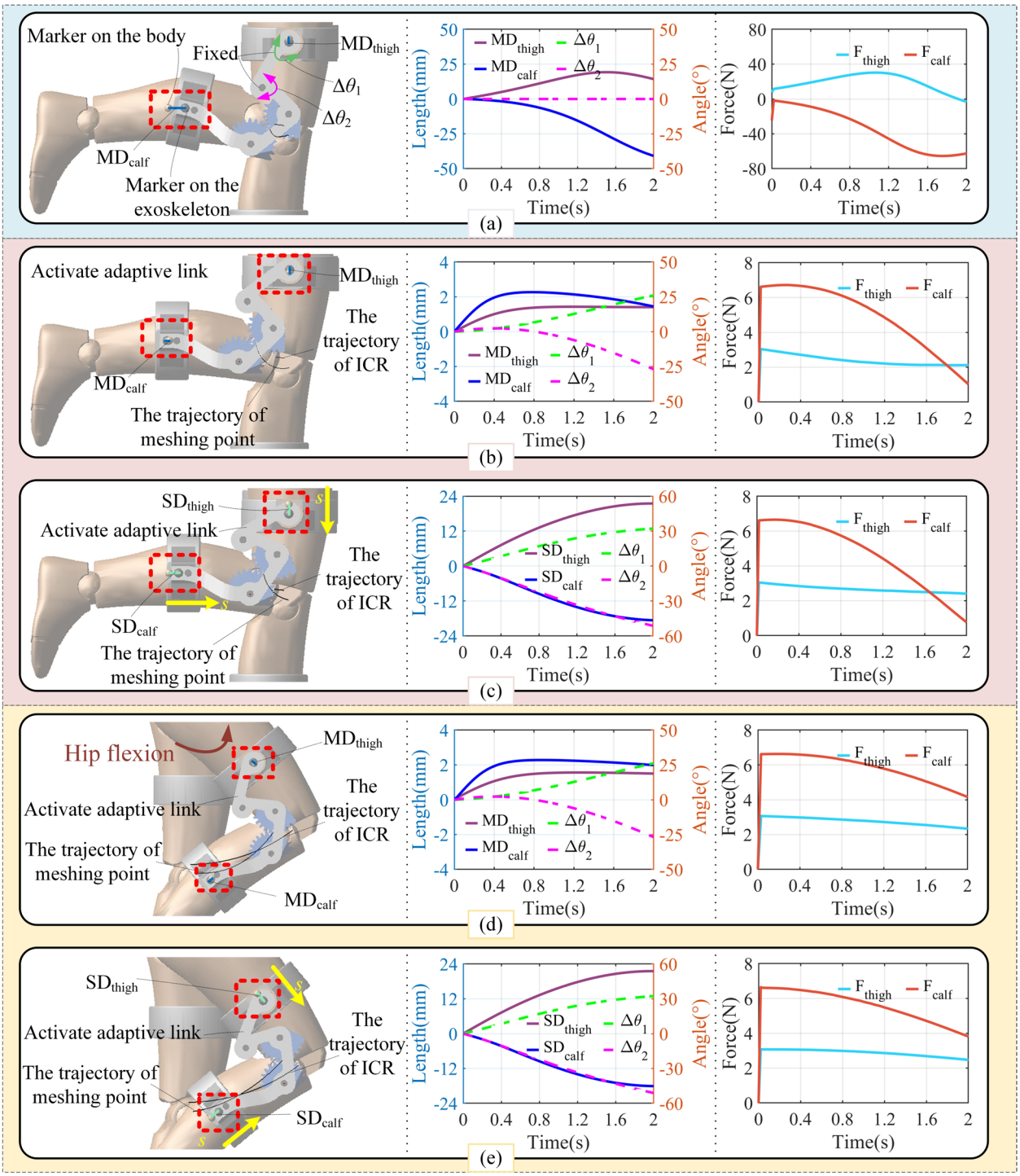

Figure 14 Simulation of MD absorption: **a** Failure adaptive link, simulating the generation of MD, **b** The simulation of activating the adaptive link, **c** Activate the adaptive link, the straps sliding on the calf and thigh, **d** Activate the adaptive link and the hip flexion, **e** Activate the adaptive link, hip flexion, and the straps sliding on the calf and thigh

shown in Figure 14c, the exoskeleton can still assist the knee motion normally even if the exoskeleton appears to slide on the leg surface. The variations of F_{calf} and F_{thigh} are slightly different from those in simulation b, but the peaks are the same as in simulation b.

Simulation d: Activate the adaptive link. The flexion angular velocity of the hip joint is arbitrarily set to 20°/s to verify whether the exoskeleton would be affected by the motion of the hip joint during the assisting process. As shown in Figure 14d, the variation of the adaptive angles is the same as those in simulation b. The variations of MD_{calf}, MD_{thigh}, and F_{calf}, F_{thigh} are slightly different from those in simulation b. However, their peaks are the same as those in simulation b.

Simulation e: Activate the adaptive link. The SD of the exoskeleton along the leg surface is arbitrarily set to $s = 20\sin(\pi t/4)$ mm, and the flexion angular velocity of the hip joint is arbitrarily set to 20 °/s. The sliding of the exoskeleton and the motion of the hip joint are combined to validate the adaptive capability of the exoskeleton. As shown in Figure 14e, the changes in F_{calf} and F_{thigh} are slightly different from those in simulation b, but the peaks are the same as in simulation b.

Through the above series of simulations, it is shown that:

(1) After adding the adaptive link, although there has always been a misalignment of the rotation axis between the exoskeleton and the human knee joint, the MD caused by the misalignment of the rotation axis can be absorbed by the adaptive joint of the adaptive link in the exoskeleton. And the force of the exoskeleton on the calf and thigh along the leg surface direction is significantly reduced, indicating that the proposed adaptive knee joint exoskeleton is an effective solution to solve the MD.

(2) The assistance of the exoskeleton to the knee joint can cope with the impact of human hip joint movement

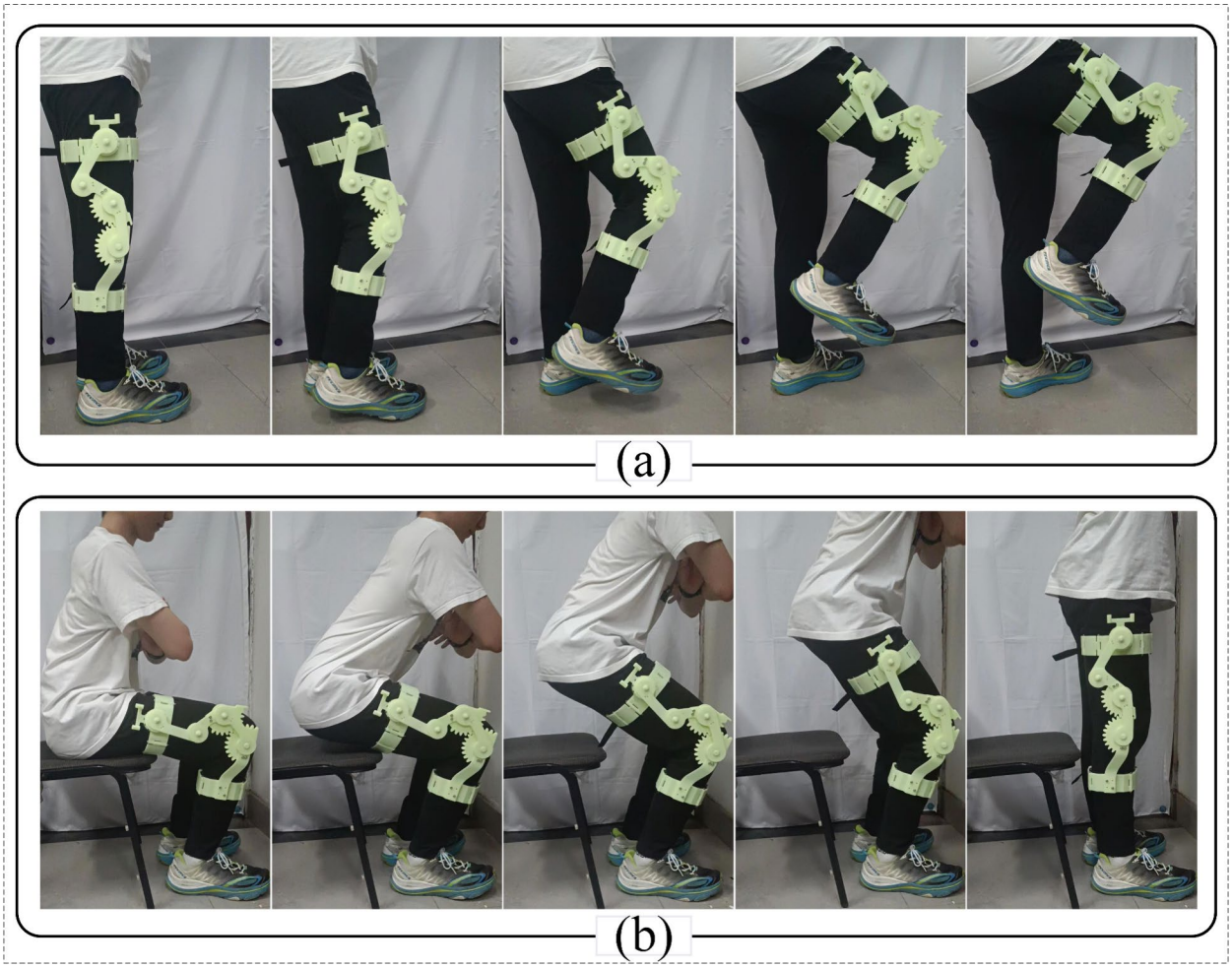

Figure 15 Kinematic compatibility test: **a** Step motion, **b** Sit-to-stand motion

and the impact of exoskeletons sliding on the human body, indicating that the proposed adaptive exoskeleton has good adaptive ability.

6.2 Verification of Human-machine Kinematic Compatibility

To verify the compatibility of human-machine kinematics, we built an unpowered mechanism principle prototype. And tests were conducted on human body wearing exoskeletons for stepping and sitting-to-standing motions.

During the process of wearing the exoskeleton, we align the designed WA with the wearer's knee joint rotation center in the sagittal plane. As shown in Figure 15, the wearer can achieve step and sit-to-stand motions without obstruction, demonstrating that the designed exoskeleton has good human-machine kinematic compatibility.

7 Conclusions

In this paper, we designed a wearable adaptive knee exoskeleton based on GLM and analyzed the proposed knee exoskeleton from the kinematic perspective. The conclusions drawn are as follows.

(1) The adaptive structural design of virtualizing the human femur, tibia, and knee joint as a part of GLM can solve the problem of misalignment of the rotational axis of the human-machine joints at the knee joint. The proposed WA helps to align the rotation axis of the human-machine joints during wearing, enhancing the convenience of aligning the rotation axis of the human-machine joints.

(2) A kinematic model of GLM was established, taking into account the changes in the ICR of the knee joint. The high consistency between theoretical and simulation values proves the correctness of the kinematic model.

(3) In order to improve the wearability of the exoskeleton, the NSGA-II optimization algorithm was used to optimize the size of the exoskeleton mechanism. The optimization results showed that the WA of the exoskeleton mechanism on the human body increased by 18.40% after optimization. The AVTR and AISS of the exoskeleton mechanism in the WA increased by 4.98% and 6.01%, respectively.

(4) The simulation of the absorption of MD by the exoskeleton demonstrates the feasibility of the proposed adaptive knee joint exoskeleton scheme and the good adaptive ability of the exoskeleton. The proposed adaptive exoskeleton has been verified to have good human-machine kinematic compatibility through motion testing after wearing exoskeletons on the human body.

In the future, we will continue to improve the engineering design of this adaptive exoskeleton. And conduct dynamic modeling and build a controller to verify the performance of the adaptive exoskeleton in terms of assistance, while also verifying the exoskeleton's performance in reducing undesired forces caused by misalignment during the assistance process.

Acknowledgements
Not applicable.

Author Contributions
XY wrote the manuscript; SG, PW, YW, LN, and DL assisted with sampling and laboratory analyses. All authors read and approved the final manuscript.

Funding
Supported by National Natural Science Foundation of China (Grant No. 52275004), Beijing Municipal Natural Science Foundation (Grant No. 3242012).

Data availability
The datasets supporting the conclusions of this article are included within the article.

Declarations

Competing Interests
The authors declare no competing financial interests.

Author Details
[1]School of Mechanical, Electronic and Control Engineering, Beijing Jiaotong University, Beijing 100044, China. [2]Key Laboratory of Vehicle Advanced Manufacturing, Measuring and Control Technology, Ministry of Education, Beijing Jiaotong University, Beijing 100044, China.

Received: 30 November 2023 Revised: 24 July 2024 Accepted: 29 July 2024
Published online: 20 September 2024

References

[1] C Q Tan, F C Sun, B Fang, et al. Autoencoder-based transfer learning in brain–computer interface for rehabilitation robot. *International Journal of Advanced Robotic Systems,* 2019, 16(2): 12.
[2] J M Zhou, S Yang, Q Xue, et al. Lower limb rehabilitation exoskeleton robot: A review. *Advances in Mechanical Engineering,* 2021, 13(4): 1-17.
[3] D Shi, W X Zhang, W Zhang, et al. A review on lower limb rehabilitation exoskeleton robots. *Chinese Journal of Mechanical Engineering,* 2019, 32(1): 11.
[4] A H A Stienen, E E G Hekman, F C T van der Helm, et al. Self-aligning exoskeleton axes through decoupling of joint rotations and translations. *IEEE Transactions on Robotics,* 2009, 25(3): 628-633.
[5] N Jarrasse, G Morel. Connecting a human limb to an exoskeleton. *IEEE Transactions on Robotics,* 2012, 28(3): 697-709.
[6] S V Sarkisian, M K Ishmael, G R Hunt, et al. Design, development, and validation of a self-aligning mechanism for high-torque powered knee exoskeletons. *IEEE Transactions on Medical Robotics and Bionics,* 2020, 2(2): 248-259.
[7] S V Sarkisian, M K Ishmael, T Lenzi. Self-aligning mechanism improves comfort and performance with a powered knee exoskeleton. *IEEE Transactions Neural Systems and Rehabilitation Engineering,* 2021, 29: 629-640.
[8] R Mallat, M Khalil, G Venture, et al. Human-exoskeleton joint misalignment: a systematic review. *Proceedings of the 5th International Conference on Advances in Biomedical Engineering (ICABME),* Tripoli, Lebanon, October 17–19, 2019: 12-15.

[9] S Y Yu, T H Huang, A Di Lallo, et al. Bio-inspired design of a self-aligning, lightweight, and highly-compliant cable-driven knee exoskeleton. *Frontiers in Human Neuroscience,* 2022, 16: 1018160.
[10] H Iwaki, V Pinskerova, M A R Freeman. Tibiofemoral movement 1: the shapes and relative movements of the femur and tibia in the unloaded cadaver knee. *Journal of Bone and Joint Surgery-British Volume,* 2000, 82B(8): 1189-1195.
[11] H Kawamoto, Y Sankai. Power assist method based on phase sequence driven by interaction between human and robot suit. *Proceedings of the 13th IEEE International Workshop on Robot and Human Interactive Communication*, Kurashiki, Japan, September 20–22, 2004: 491–496.
[12] H Kazerooni, J L Racine, L H Huang. On the control of the Berkeley lower extremity exoskeleton (BLEEX). *Proceedings of the IEEE International Conference on Robotics and Automation (ICRA),* Barcelona, SPAIN, April 18-22, 2005: 4353–4360.
[13] K Suzuki, G Mito, H Kawamoto. Intention-based walking support for paraplegia patients with robot suit HAL. *Advanced Robotics,* 2007, 21(12): 1441-1469.
[14] K A Strausser, T A Swift, A B Zoss. Prototype medical exoskeleton for paraplegic mobility: First experimental results. *Proceedings of the ASME Dynamic Systems and Control Conference*, Cambridge, MA, September 12–15, 2010: 453–458.
[15] K A Strausser, H Kazerooni. The development and testing of a human machine interface for a mobile medical exoskeleton. *Proceedings of the IEEE International Conference on Intelligent Robots and Systems*, San Francisco, CA , September 25-30, 2011: 4911–4916.
[16] G Zeilig, H Weingarden, M Zwecker. Safety and tolerance of the ReWalk (TM) exoskeleton suit for ambulation by people with complete spinal cord injury: A pilot study. *Journal of Spinal Cord Medicine,* 2012, 35(2): 96-101.
[17] T Kim, M Jeong, K Kong, et al. Bioinspired knee joint of a lower-limb exoskeleton for misalignment reduction. *IEEE/ASME Transactions on Mechatronics,* 2022, 27(3): 1223-1232.
[18] J L Wang, X Li, T-H Huang, et al. Comfort-centered design of a lightweight and backdrivable knee exoskeleton. *IEEE Robotics and Automation Letters,* 2018, 3(4): 4265-4272.
[19] J-H Kim, M Shim, D H Ahn, et al. Design of a knee exoskeleton using foot pressure and knee torque sensors. *International Journal of Advanced Robotic Systems,* 2015, 12(8): 14.
[20] M Lyu, W Chen, X Ding, et al. Design of a biologically inspired lower limb exoskeleton for human gait rehabilitation. *Review of Scientific Instruments,* 2016, 87(10): 104301.
[21] G M Bapat, S Sujatha. A method for optimal synthesis of a biomimetic four-bar linkage knee joint for a knee-ankle-foot orthosis. *Journal of Biomimetics, Biomaterials and Biomedical Engineering,* 2017, 32: 20-28.
[22] M Olinski, A Gronowicz, M Ceccarelli. Development and characterization of a controllable adjustable knee joint mechanism. *Mechanism and Machine Theory,* 2021, 155: 104101.
[23] S Jun, X B Zhou, D K Ramsey, et al. Compliant knee exoskeleton design: parallel coupled compliant plate (PCCP) mechanism and pennate elastic band (PEB) spring. *Proceedings of the ASME Design Engineering Technical Conferences and Computers and Information in Engineering Conference (DETC),* Buffalo, New York, USA, August 17–20, 2014.
[24] S Jun, X B Zhou, D K Ramsey, et al. Smart knee brace design with parallel coupled compliant plate mechanism and pennate elastic band spring. *Journal of Mechanisms and Robotics,* 2015, 7(4): 041024.
[25] D B Sui, B-C Chang, R Hidayah, et al. SpringExo, a spring-based exoskeleton for providing knee assistance: design, characterization and feasibility study. *Proceedings of the 2021 IEEE International Conference on Robotics and Automation (ICRA)*, Xi'an, China, May 31 - June 4, 2021: 10513-10519.
[26] B Celebi, M Yalcin, V Patoglu. Assiston-knee: A self-aligning knee exoskeleton. *Proceedings of the 2013 IEEE/RSJ International Conference on Intelligent Robots and Systems (IROS)*, Tokyo, Japan, November 3-7, 2013: 996–1002.
[27] B Choi, Y Lee, J Kim, et al. A self-aligning knee joint for walking assistance devices. *Proceedings of the 38th Annual International Conference of the IEEE Engineering in Medicine and Biology Society (EMBC)*, Orlando, FL, August 16-20, 2016: 2222–2227.
[28] Y Lee, Y-J Kim, J Lee, et al. Biomechanical design of a novel flexible exoskeleton for lower extremities. *IEEE/ASME Transactions on Mechatronics,* 2017, 22(5): 2058-2069.
[29] B Choi, Y Lee, Y-J Kim, et al. Development of adjustable knee joint for walking assistance devices. *Proceedings of the 2017 IEEE/RSJ International Conference on Intelligent Robots and Systems (IROS)*, Vancouver, BC, Canada, September 24–28, 2017: 1790–1797.
[30] Y Lee, J Lee, B Choi, et al. Flexible gait enhancing mechatronics system for lower limb assistance (GEMS L-Type). *IEEE/ASME Transactions on Mechatronics,* 2019, 24(4): 1520-1531.
[31] B Choi, Y Lee, J Lee, et al. Development of adjustable knee assist device for wearable robot based on linkage and rolling joint. *Proceedings of the 2019 IEEE/RSJ International Conference on Intelligent Robots and Systems (IROS)*, Macau, China, November 4-8, 2019:4043–4050.
[32] H W Li, D B Sui, H T Ju, et al. Mechanical compliance and dynamic load isolation design of lower limb exoskeleton for locomotion assistance. *IEEE/ASME Transactions on Mechatronics,* 2022, 27(6): 5392-5402.
[33] D A Neumann. Kinesiology of the musculoskeletal system: foundations for rehabilitation (Second Edition). St Louis, MO: Mosby, 2010.
[34] P S Walker, H Kurosawa, J S Rovick, et al. External knee joint design based on normal motion. *Journal of Rehabilitation Research and Development,* 1985, 22(1): 9-22.
[35] J M Baydal Bertomeu, J M Belda Lois, R Barbera Guillem, et al. Development of a hinge compatible with the kinematics of the knee joint. *Prosthetics and Orthotics International,* 2007, 31(4): 371-383.
[36] G T Li, L Cheng, N Sun. Design, manipulability analysis and optimization of an index finger exoskeleton for stroke rehabilitation. *Mechanism and Machine Theory,* 2022, 167:104526.
[37] K Deb, A Pratap, S Agarwal, et al. A fast and elitist multiobjective genetic algorithm: NSGA-II. *IEEE Transactions on Evolutionary Computation,* 2022, 6(2): 182-197.

Xinhua Yang born in 1999, is currently a PhD candidate at *School of Mechanical, Electronic and Control Engineering, Beijing Jiaotong University, China*. He received his bachelor's degree from *Beijing Jiaotong University, China*, in 2021. His research interests include lower limb exoskeleton robots and robotic mechanisms.

Sheng Guo born in 1972, received his Ph.D. from *Beijing Jiaotong University, China*, in 2005. He was a Visiting Scholar at *University of California, Irvine, US*, in 2010–2011. Currently, he is a Full Professor, the Vice Director of the *Robotics Institute*, and the Dean of *School of Mechanical, Electronic and Control Engineering, Beijing Jiaotong University, China*. His research interests include robotic mechanisms and mechatronics.

Peiyi Wang born in 1995, is currently a PhD candidate at *School of Mechanical, Electronic and Control Engineering, Beijing Jiaotong University, China*. He received his bachelor's degree from *Beijing Jiaotong University, China*, in 2018. His research interests include mechanical design and control continuum robots.

Yifan Wu born in 1993, is currently a PhD candidate at the *Robotics Research Center, Beijing Jiaotong University, China*. He received his Bachelor's degree from the *Beijing Jiaotong University, China*, in 2016. In 2019, he received a Diploma in Engineering and Master's degree from the *University of Montpellier, France*. His research interests include control methods for legged robots, machine learning, and innovation of parallel mechanisms.

Lianzheng Niu born in 1994, is currently a PhD candidate at the *Robotics Research Center, Beijing Jiaotong University, China*. He received his Bachelor's degree from *Henan University of Engineering, China,* in 2018. In 2021, he received his Master's degree from *North China University of Technology, China.* His research interests include robotic mechanisms and exoskeleton–parallel robots.

Duxin Liu born in 1987, is currently an associate professor at the *Robotics Institute, Beijing Jiaotong University, China*. He received his Ph.D. from the *University of Chinese Academy of Sciences, China*, in 2018. His research interests include human-robot fusion exoskeleton robots and robotized railway equipment.